PERGAMON

International Journal of Heat and Mass Transfer 42 (1999) 4375–4389

International Journal of HEAT and MASS TRANSFER

www.elsevier.com/locate/ijhmt

Solidification inside an axially rotating pipe containing a turbulent liquid flow

K.-J. Rinck, H. Beer*

Institut für Technische Thermodynamik, Technische Universität Darmstadt, Petersenstr. 30, 64287 Darmstadt, Germany

Received 29 September 1998; received in revised form 19 February 1999

Abstract

This paper presents an experimental and a numerical method to analyze the formation of the steady-state solid–liquid interface in a cooled axially rotating pipe for turbulent flow and constant wall temperature.

The experimental investigations show that wavy ice layers occur when the fluid acceleration due to growth of the solid phase is strong enough to cause a flow laminarization. The comparison of the experiments with the numerical calculations reveals that the applied Reynolds stress turbulence closure is able to capture the effects caused by the acceleration as well as the laminarization due to flow rotation.

1. Introduction

Freezing in liquid flow inside tubes is an important engineering problem occurring in the field of water transport in cold regions and in the field of casting, among others. For steady-state conditions and constant wall temperature Zerkle and Sunderland [1] solved the problem of the laminar flow analytically. They assumed a parabolic axial velocity distribution throughout the full length of the cooled section.

The solidification in turbulent pipe and channel flows was investigated numerically by Weigand and Beer [2], applying Prandtl's mixing length hypothesis. The calculations were restricted to smooth ice layers with a monotonously increasing thickness in flow direction. Gilpin's [3] experimental investigations of the turbulent pipe flow revealed that for sufficiently high freezing parameters and low Reynolds numbers the acceleration of the fluid due to the converging ice layer causes a flow laminarization and a reduction of the heat transfer rate in the entrance region of the cooled section followed by a retransition to full turbulent flow. This leads to a wavy ice structure, frequently migrating a certain distance upstream. Further experiments concerning the formation of wavy ice layers are known by Hirata and Matsuzawa [4]. Assuming a constant turbulent shear stress along the streamlines in the strongly accelerating part of a cooled channel flow, Weigand and Beer [5] calculated wavy ice layers which are in good agreement with their own experimental results.

The flow in an axially rotating pipe arising frequently in the field of rotating machineries is also an important engineering problem. Kikuyama et al. [6] investigated the influence of the pipe rotation on the flow field experimentally and theoretically. For turbulent entrance flow they observed a laminarization of the axial velocity distribution and a reduced hydraulic loss in comparison with the non-rotating pipe flow. Reich and Beer [7] examined the same kind of flow with special regard to the heat transfer rate and observed that the flow laminarization causes a reduction of the Nusselt number, too. Nishibori et al. [8] considered the radial distribution of the streamwise velocity fluctuations along the developing turbulent

* Corresponding author.

0017-9310/99/$ - see front matter
PII: S0017-9310(99)00095-2

Nomenclature

A	stress flatness factor, Eq. (27)
A_2, A_3	second and third invariants of a_{ij}
a	thermal diffusivity
a_{ij}	dimensionless anisotropic Reynolds stress, Eq. (20)
B	dimensionless freezing parameter, $\Theta_C k_s/k_l$
C_{ij}	convective transport of $\overline{v_i v_j}$
D	pipe diameter
d_{ij}	turbulent diffusive transport of $\overline{v_i v_j}$
K	acceleration parameter, Eq. (1)
k	turbulent kinetic energy, $\overline{v_k v_k}/2$
k_l, k_s	thermal conductivity of the liquid and the solid phase, respectively
N	rotation rate, $V_{\varphi W}/V_{z0}$
N_l	local rotation rate, $N(\delta/R)^3$
n_i	unit vector perpendicular to the surface
P	time mean pressure
Pr	Prandtl number, ν/a
Pr_t	turbulent Prandtl number, ν_t/ν_q
P_{ij}	shear generation rate of $\overline{v_i v_j}$
P_k	shear generation rate of k, $P_{kk}/2$
p	pressure fluctuations
R	pipe radius
R_{ij}	additional components in the equations for $\overline{v_i v_j}$ arising due to the coordinate transformation
Re_D	Reynolds number at the entrance, $V_{z0}D/\nu$
Re_l	local Reynolds number, $V_{zl}2\delta/\nu$
Re_t	turbulent Reynolds number, $k^2/(\epsilon\nu)$
r	radial coordinate
$\tilde{r}$	scaled dimensionless radial coordinate, r/δ
T	time mean temperature
T_F	freezing temperature of the liquid
V_i	time mean velocity in direction i
V_{z0}	mean axial velocity over the pipe cross section at the entrance
V_{zl}	mean axial velocity over the local pipe cross section, $V_{z0}(R/\delta)^2$
v_i	velocity fluctuation in direction i
$\overline{v_i t}$	turbulent heat flux in direction i
$\overline{v_i v_j}$	kinematic Reynolds stress
x_i	cartesian coordinate in direction i
z	axial coordinate
z_w	position of the flow separation point.

Greek symbols

δ	free pipe radius
δ_{ij}	Kronecker's symbol
ϵ	dissipation rate of turbulence energy
$\tilde{\epsilon}$	modified dissipation rate of turbulence energy, Eq. (35)
ϵ_{ij}	kinematic dissipation rate of $\overline{v_i v_j}$
Θ_C	dimensionless cooling temperature ratio, $(T_F - T_W)/(T_0 - T_F)$
ν	kinematic viscosity
ν_q	turbulent thermal diffusivity
ν_t	eddy viscosity
ν_{ij}	viscous diffusion of $\overline{v_i v_j}$
ρ	density
Φ_{ij}	pressure–strain correlation
φ	tangential coordinate
ω	angular frequency.

Subscripts

s	solid phase
W	at the pipe wall
0	at the entrance.

flow in a rotating pipe. Compared with the flow without swirl they observed, especially in the entrance region, a considerable decrease of the streamwise velocity fluctuations.

Weigand and Beer [9] calculated the turbulent rotational entrance flow numerically by using a mixing length hypothesis. In order to take into account the influence of streamline curvature they introduced the Richardson number as a parameter of the mixing length. The tangential velocity distribution along the rotating section was given by an empirical, but universal correlation. Hirai et al. [10] showed that a standard eddy viscosity turbulence model fails to predict correctly the fully developed flow in an axially rotating pipe, whereas a Reynolds stress turbulence closure is able to capture the laminarization effect influencing the axial velocity field as well as the universally observed parabolic tangential velocity distribution. For the same kind of flow Eggels [11] applied a large eddy simulation successfully.

The formation of the solid phase in a cooled axially rotating pipe at low flow-rate Reynolds numbers was investigated theoretically by Rinck and Beer [12], applying a zero-equation turbulence model. As far as we know there exist no experimental data concerning the freezing in an axially rotating pipe flow whose technical application can be found in the field of centrifugal casting.

2. Experiment

2.1. Experimental apparatus

A schematic outline of the horizontally mounted apparatus is shown in Fig. 1. It mainly consists of a test section, a refrigeration unit and two circulation systems for water and coolant, respectively.

Water is pumped from a tank through an insulated calming section, 2.6 m in length, in order to ensure a fully developed non-rotating turbulent flow at the entrance of the test section. The temperature of the water is measured with three thermocouples at the inlet and controlled by an NTC (temperature dependant resistor) controlled heater.

The test section is constructed of two concentric tubes with an arrangement of bearings and rotary shaft seals. The water flows through the cooled inner brass tube which has a 50 mm i.d. and rotates around its axis. Pipe rotation is accomplished by a variable speed d.c. motor and a V-belt drive. The temperature of the rotating pipe wall is measured by 11 thermocouples. With the aid of a slip ring the thermoelectric voltages are transmitted to the stationary instrumentation.

Cooling is provided by an ethylene glycol–water mixture circulating with high velocity through the narrow annulus between the tubes which is divided into 10 chambers. In order to enhance heat transfer, spiral ripples were welded on the outer surface of the rotating pipe. The coolant flow loop consists of the refrigeration unit with an integrated pump, a coolant distributor and collector as well as thermometric measuring instruments. This loop can be switched over to a second loop with 'warm coolant' for melting the ice layer frozen at the inner surface of the tube. This is necessary in order to remove the solid phase from the apparatus for observation and thickness-measurement at the end of the experiment.

2.2. Operating procedure

During the experiment the water flow rate, the rotational speed of the pipe, the inlet temperature, the temperature of the coolant and the wall temperature of the rotating pipe are controlled. The stationary case is considered to be found when all wall temperatures which are slightly influenced by the formation and the migration of the ice-waves do not change for at least two hours. Then, the water pump and the d.c. motor are switched off in order to generate a second ice layer coating the inner surface of the solid phase that developed during the experiment.

After 10 min, when the liquid core in the test section

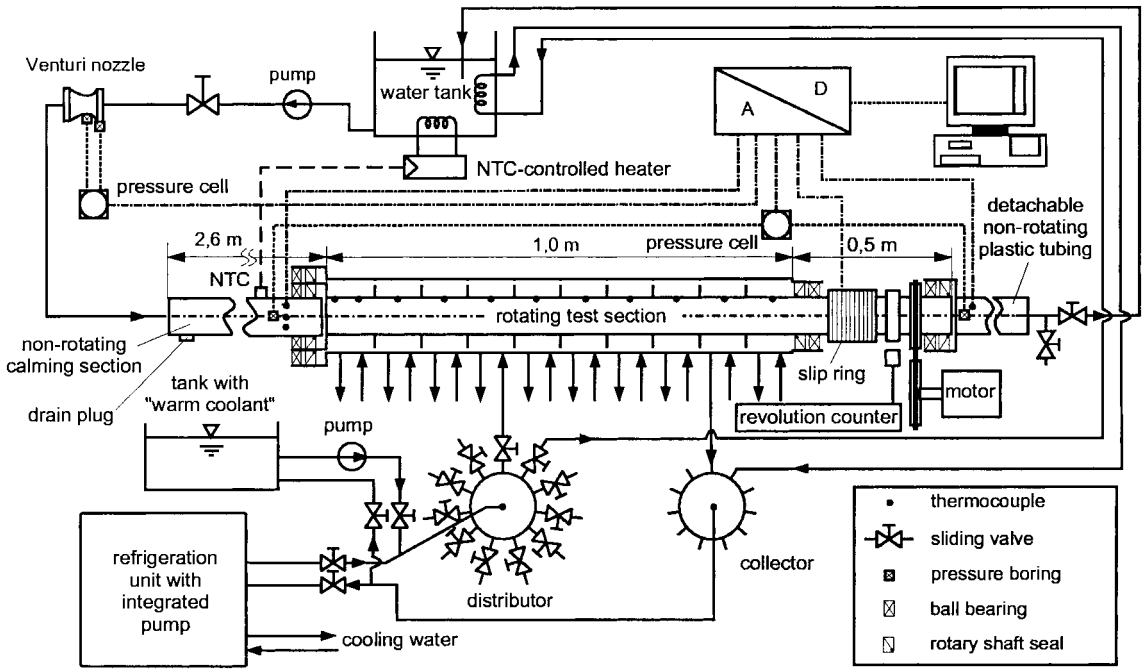

Fig. 1. Schematic drawing of experimental apparatus.

has a diameter of about 2 cm yet, the tube is drained off and the plastic tubing at the end of the pipe is detached from the bearing block (see Fig. 1). After that, a thin plastic tube, 2 m in length and with 1 cm o.d., is slipped through the opening into the test section. The water loop is closed again and the pipe is filled with water by switching on the pump for a few seconds. The described coating of the investigated ice layer avoids a damage of same during this procedure.

In the next 30 min the pipe freezes up completely while the thin plastic tube in the test section ensures that no tension is imposed on the ice structure. Finally, the outer surface of the ice cylinder is melted slightly by switching over to the loop with the 'warm coolant' and the entire ice structure is removed from the apparatus by detaching the big plastic tubing once again and pulling out the thin tube.

Because of the curved cylinder surface the optical distortion is considerable and the developed ice layer can not be observed directly. Thus, it is put into a rectangular acrylic basin filled with cold water that has almost the same refractive index like ice. Now it is possible to record the ice layer photographically with only a slight distortion which can be taken into account by calculation. Due to the different morphology of the ice developed slowly during the experiment and the ice generated rapidly afterwards, the shape of the frozen crust is easy to make out.

3. Experimental results

The range of conditions employed in the present investigations are:

- Reynolds number Re_D: $5000 \leq Re_D \leq 40{,}000$
- Rotation rate N: $0 \leq N \leq 1$
- Inlet temperature T_0: $274.5\ \mathrm{K} \leq T_0 \leq 277.2\ \mathrm{K}$
- Wall temperature T_W: $262\ \mathrm{K} \leq T_W \leq 268\ \mathrm{K}$

Therefore, the cooling temperature ratio $\Theta_C = (T_F - T_W)/(T_0 - T_F)$ varies in the range $1.2 \leq \Theta_C \leq 7.3$.

In the following the effects influencing the flow, the heat transfer and, finally, the shape of the solid phase are described.

3.1. Laminarization due to flow acceleration and pipe rotation

Because the cross section of flow depends on the free pipe radius δ squared (see Fig. 9), even a thin ice layer causes a considerable flow acceleration in the entrance region of the test section. Its intensity can be described by the acceleration parameter

$$K = \frac{\nu}{V_{z1}^2}\frac{\mathrm{d}V_{z1}}{\mathrm{d}z} = -\frac{4}{Re_D}\frac{\delta}{R}\frac{\mathrm{d}\delta}{\mathrm{d}z} \tag{1}$$

which takes extremely high values up to 50×10^{-6} in the present study. Moretti and Kays [13] found that a flow laminarization already occurs for $K = 2 \div 3 \times 10^{-6}$. Therefore, a strong suppression of the turbulent fluctuations takes place which reduces the convective heat transfer in this region. As a result the local ice layer thickness increases amplifying the flow acceleration again. This occurrence is damped by the increase of the local Reynolds number $Re_1 = Re_D R/\delta$ enhancing the turbulence.

Downstream the ice layer thickness does not change much any more in flow direction and the flow acceleration dies off rapidly. This introduces the retransition of the laminarized flow to an again full turbulent flow causing a wavy shape of the solid phase. In some cases this procedure repeats itself and ice layers with several waves can be observed.

The pipe rotation leads to a laminarization of the turbulent flow and reduces the convective heat transfer in the fluid, too. But, in contrast to the flow acceleration, the local rotation rate

$$N_1 = \frac{V_\varphi\,|_{r=\delta}}{V_{z1}} = \frac{V_{\varphi W}\dfrac{\delta}{R}}{V_{z0}\left(\dfrac{R}{\delta}\right)^2} = N\left(\frac{\delta}{R}\right)^3 \tag{2}$$

and, therefore, the influence of the rotation decreases rapidly when the solid phase becomes thicker.

3.2. Classification of ice structure

Figs. 2 and 3 show the two different kinds of waves observed in the experiments [4,14]. A 'smooth transition' denotes a wave without flow separation occurring when the ice layer is thin and the suppression of the turbulence due to the converging duct is moderate. In contrast to this, a 'step transition' develops if the solid phase is thick enough to cause an intensive flow laminarization. In this case the flow separates at the point where the ice layer has its maximum thickness, inducing the mentioned upstream migration of the wave.

In our experiments with a non-rotating pipe (see Fig. 4) a 'smooth transition' can be observed when the cooling temperature is lower than

$$\Theta_C\,|_{N=0} = 0.0038\,Re_D^{2/3}. \tag{3}$$

Because the rotation leads to an increase of the ice layer thickness this limit is reduced to

$$\Theta_C\,|_{N=0.5} = 2.4 \times 10^{-4}\,Re_D^{11/12} \tag{4}$$

for a pipe rotating with $N = 0.5$ (see Fig. 5).

The stationary separation point of the 'step transition' ice formation z_w can be correlated with a maxi-

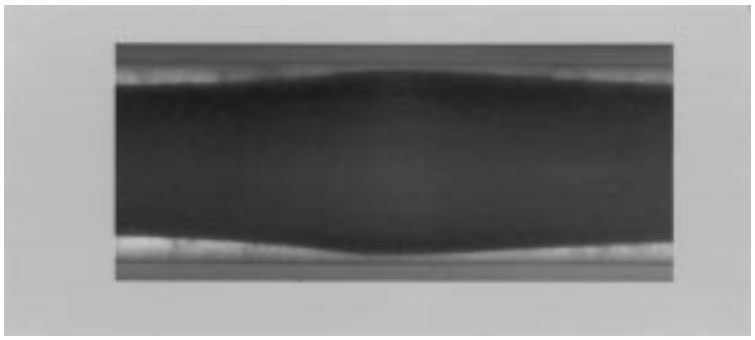

Fig. 2. 'Smooth transition'.

mum error of less than 20% by

$$\left.\frac{z_w}{D}\right|_{N=0} = 797 Re_D^{-0.29} B^{-1} \tag{5}$$

in the non-rotating pipe and by

$$\left.\frac{z_w}{D}\right|_{N=0.5} = 29.78 B^{-0.94} \tag{6}$$

for $N = 0.5$. Eqs. (5) and (6) show that an increase of the cooling parameter as well as the pipe rotation lead to a separation point located closer to the entrance and reduce the spacing between the separation points causing ice layers with several waves, too (see Figs. 6–8).

4. Analysis

4.1. Basic equations

Fig. 9 illustrates the geometry of the considered problem. The fluid enters the cooled section at $z = 0$ with a fully developed turbulent non-rotating flow and with the constant temperature T_0. In the chill region ($z > 0$) the temperature of the pipe wall is kept at a constant value T_W which is lower than the freezing temperature of the fluid T_F and, therefore, a solid phase is generated at the cooled wall.

On the assumption that free convection effects are negligible the time mean conservation equations of mass, momentum and energy in cartesian coordinates for a steady-state flow of a Newtonian fluid with constant properties can be reduced to

$$\frac{\partial V_j}{\partial x_j} = 0, \tag{7}$$

$$V_j \frac{\partial V_i}{\partial x_j} = -\frac{1}{\rho}\frac{\partial P}{\partial x_i} + \nu \frac{\partial^2 V_i}{\partial x_j \partial x_j} - \frac{\partial \overline{v_i v_j}}{\partial x_j}, \tag{8}$$

$$V_i \frac{\partial T}{\partial x_i} = a \frac{\partial^2 T}{\partial x_i \partial x_i} - \frac{\partial \overline{v_i t}}{\partial x_i}. \tag{9}$$

The transport equations of the Reynolds stresses can be written as

$$C_{ij} = P_{ij} + \nu_{ij} + \Phi_{ij} + d_{ij} - \epsilon_{ij} + R_{ij}. \tag{10}$$

In these equations

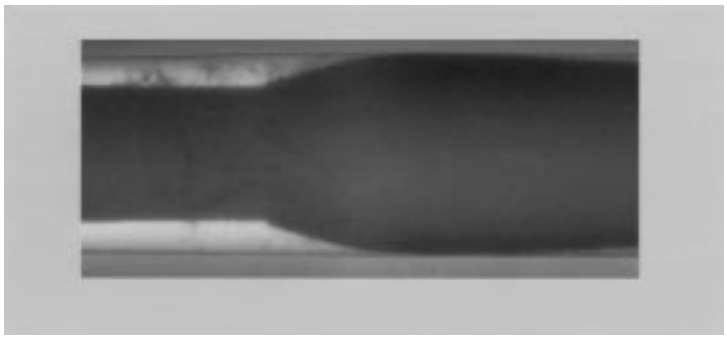

Fig. 3. 'Step transition'.

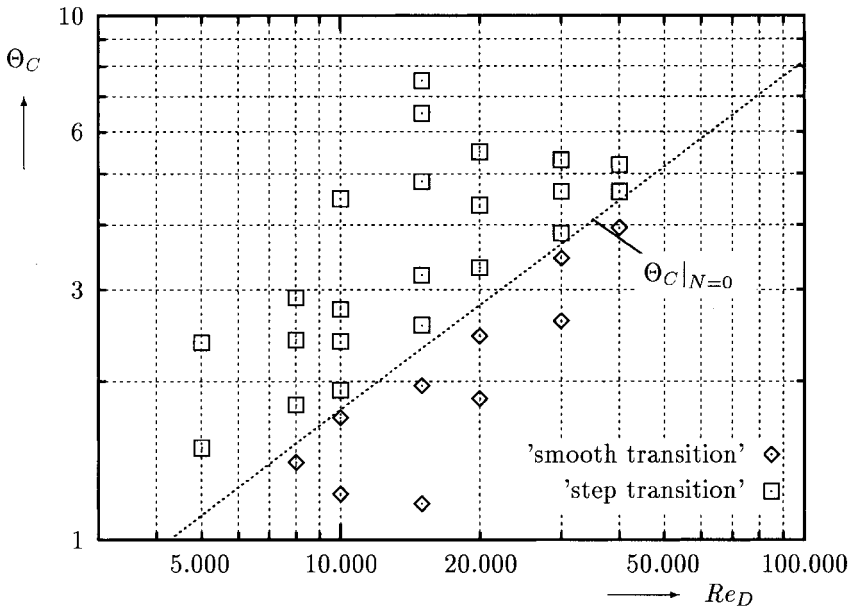

Fig. 4. Logarithmic Re_D–Θ_C diagram for $N = 0$.

$$C_{ij} \equiv V_k \frac{\partial \overline{v_i v_j}}{\partial x_k} \tag{11}$$

are the convection terms,

$$P_{ij} \equiv -\left[\overline{v_i v_k}\frac{V_j}{x_k} + \overline{v_j v_k}\frac{V_i}{x_k}\right] \tag{12}$$

is the stress generation rate by mean shear,

$$\nu_{ij} \equiv \frac{\partial}{\partial x_k}\left(\nu \frac{\partial \overline{v_i v_j}}{\partial x_k}\right) \tag{13}$$

the viscous diffusion,

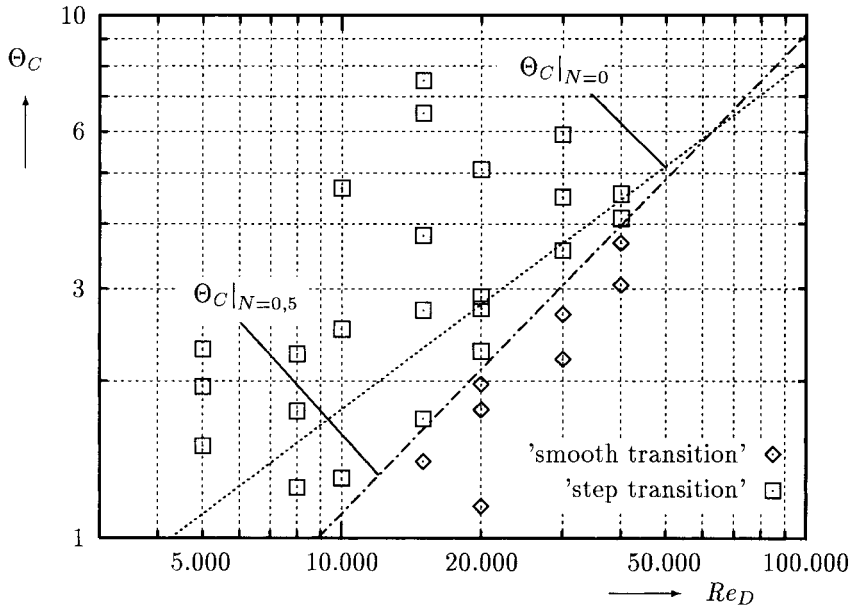

Fig. 5. Logarithmic Re_D–Θ_C diagram for $N = 0.5$.

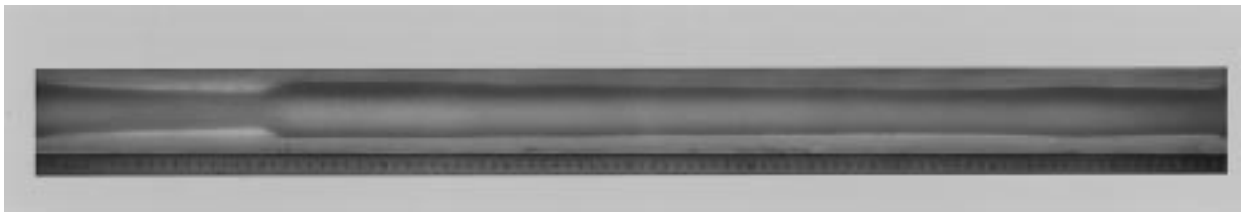

Fig. 6. Ice layer with two waves at $Re_D = 10{,}000$, $B = 10$, $N = 0.5$.

$$\Phi_{ij} \equiv \overline{\frac{p}{\rho}\left(\frac{\partial v_i}{\partial x_j} + \frac{\partial v_j}{\partial x_i}\right)} \tag{14}$$

the pressure–strain correlation,

$$d_{ij} \equiv -\frac{\partial}{\partial x_k}\left(\overline{v_i v_j v_k} + \frac{1}{\rho}\overline{p v_i}\delta_{jk} + \frac{1}{\rho}\overline{p v_j}\delta_{ik}\right) \tag{15}$$

the turbulent diffusion and

$$\epsilon_{ij} \equiv 2\nu\overline{\frac{\partial v_i}{\partial x_k}\frac{\partial v_j}{\partial x_k}} \tag{16}$$

the dissipation rate.

A further simplification is achieved by the fact that the rotating pipe flow is axisymmetric and by the common boundary layer assumptions [15] leading to a parabolic type of the governing equations.

The transformation from the Cartesian into the cylindrical coordinate system causes additional terms in the momentum equations, known as the centrifugal and the Coriolis force. Moreover, comprehensive additional terms

$$R_{ij} = P_{ij,\,\mathrm{add}} + \nu_{ij,\,\mathrm{add}} - C_{ij,\,\mathrm{add}} + \Phi_{ij,\,2,\,\mathrm{add}} + d_{ij,\,\mathrm{add}} \tag{17}$$

arise in the transport equations for the Reynolds stresses, too [10,16,17].

4.2. Turbulence model

In the transport equations of the Reynolds stresses the pressure-strain correlation Φ_{ij}, the turbulent diffusion d_{ij} and the dissipation rate ϵ_{ij} have to be modelled. For the calculation of these terms a slightly modified low-Reynolds-number second-moment closure proposed by Launder and Shima [18] is applied, which has proved to be reliable for strongly accelerated as well as for highly swirling flows [16,19].

The model for the pressure–strain correlation consists of four parts:

$$\Phi_{ij} = \Phi_{ij,\,1} + \Phi_{ij,\,2} + \Phi^{w}_{ij,\,1} + \Phi^{w}_{ij,\,2} \tag{18}$$

$\Phi_{ij,1}$ is the so-called 'return-to-isotropy' part and $\Phi_{ij,2}$ represents the 'rapid' term. With $\Phi^{w}_{ij,1}$ and $\Phi^{w}_{ij,2}$ the 'echo' effects of the reflected pressure fluctuations in the vicinity of a rigid wall are taken into account. $\Phi_{ij,1}$ is modelled by the 'return-to-isotropy' model of Rotta [20]

$$\Phi_{ij,\,1} = -c_1\epsilon a_{ij}, \tag{19}$$

a_{ij} denoting the dimensionless anisotropic parts of the Reynolds stresses:

$$a_{ij} = \frac{\overline{v_i v_j}}{k} - \frac{2}{3}\delta_{ij}. \tag{20}$$

For the 'rapid' part $\Phi_{ij,2}$ Launder and Shima propose the standard isotropization of production (IP) model. But, especially in complex swirling flows, a better coincidence with experimental results can be achieved with the isotropization of production and convection (IPC) model [11,21], because the additional convective terms arising due to the coordinate transformation have a considerable influence on the turbulence in the rotating pipe flow:

$$\Phi_{ij,\,2} = -c_2\left(P_{ij} - \frac{1}{3}\delta_{ij}P_{kk} - C_{ij} + \frac{1}{3}\delta_{ij}C_{kk}\right). \tag{21}$$

The 'echo' effects are modelled by

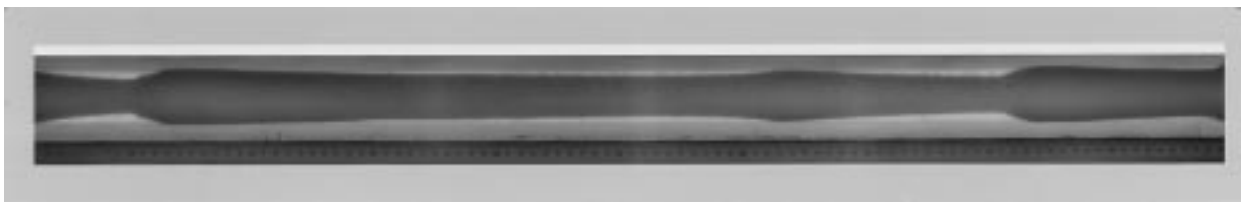

Fig. 7. Ice layer with three waves at $Re_D = 10{,}000$, $B = 18$, $N = 0.5$

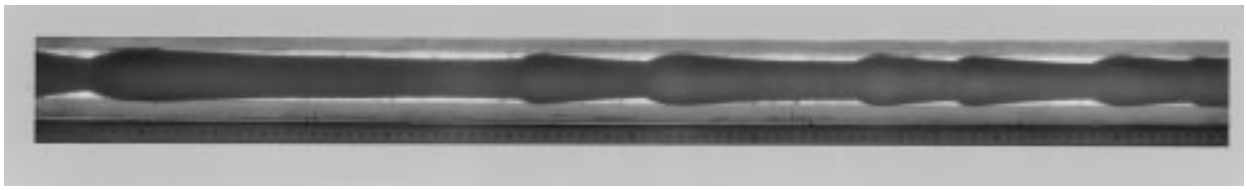

Fig. 8. Ice layer with several waves at $Re_D = 15000$, $B = 30$, $N = 0.5$.

$$\Phi^{w}_{ij,1} = c^{w}_{1}\frac{\epsilon}{k}\left(\overline{v_k v_i}n_k n_l\delta_{ij} - \tfrac{3}{2}\overline{v_k v_i}n_k n_j - \tfrac{3}{2}\overline{v_k v_j}n_k n_i\right)f_w, \quad (22)$$

$$\Phi^{w}_{ij,2} = c^{w}_{2}\left(\Phi_{kl,2}n_k n_l\delta_{ij} - \frac{3}{2}\Phi_{ik,2}n_k n_j - \frac{3}{2}\Phi_{jk,2}n_k n_i\right)f_w \quad (23)$$

with the near-wall damping function

$$f_w = 0.4\frac{k^{3/2}}{\epsilon x_2}, \quad (24)$$

x_2 being the distance normal to the wall.

The extension of the turbulence model to the viscous sublayer is achieved by expressing the coefficients in the pressure–strain correlation model as functions of the turbulent Reynolds number

$$Re_t \equiv \frac{k^2}{\nu\epsilon} \quad (25)$$

and the two independent Reynolds stress invariants

$$A_2 \equiv a_{kl}a_{lk}, \quad A_3 \equiv a_{kl}a_{lm}a_{mk}. \quad (26)$$

The parameter

$$A \equiv 1 - \frac{9}{8}(A_2 - A_3) \quad (27)$$

ranges from zero in the two-component limit to unity in isotropic turbulence and can be interpreted as the 'flatness' of turbulence.

The comparatively small wall effects concerning the turbulent diffusion d_{ij} are neglected and, in order to minimize the number of empirical values, Φ_{ij} is assumed to include the wall effects on the dissipation rate, too.

For the coefficients the following set of equations is employed:

$$c_1 = 1 + 2.58AA_2^{1/4}(1 - \exp[-(0.0067Re_t)^2]), \quad (28)$$

$$c_2 = 0.83\sqrt{A} \quad (29)$$

$$c^{w}_{1} = -\frac{2}{3}c_1 + 1.67, \quad (30)$$

$$c^{w}_{2} = \max\left[\left(\frac{2}{3} - \frac{1}{6c_2}\right), 0\right]. \quad (31)$$

Daly and Harlow's [22] generalized gradient diffusion hypothesis is chosen for modelling the turbulent diffusion term:

$$d_{ij} = \frac{\partial}{\partial x_k}\left(c_s\frac{k}{\epsilon}\overline{v_k v_l}\frac{\partial\overline{v_i v_j}}{\partial x_l}\right). \quad (32)$$

The calculation of the fully developed pipe flow at the entrance of the cooled section reveals too high values for the normal Reynolds stresses at the symmetry line when the standard value $c_s = 0.22$ is employed. This can be explained by the singularity in Daly and Harlow's model for $r = 0$, causing an overprediction of turbulent diffusion in the area close to the symmetry

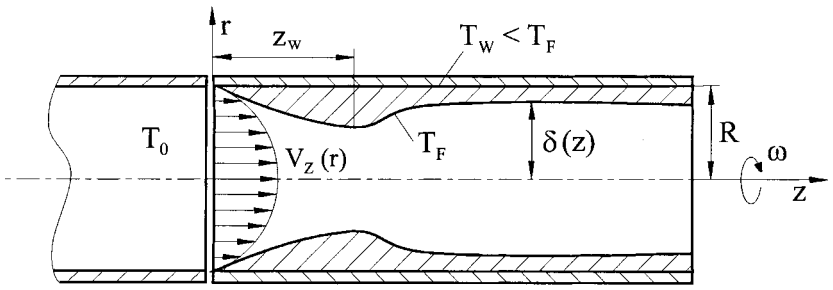

Fig. 9. Physical model.

axis. Thus, $c_s = 0.11$ is chosen providing excellent agreement with experimental results [19].

For the dissipation rate ϵ_{ij} local isotropy is assumed:

$$\epsilon_{ij} = \frac{2}{3}\delta_{ij}\epsilon. \tag{33}$$

The energy dissipation rate ϵ is calculated with the aid of the following transport equation [18]:

$$V_k \frac{\partial \epsilon}{\partial x_k} = \frac{\partial}{\partial x_k}\left[\left(c_\epsilon \frac{k}{\epsilon}\overline{v_k v_l} + \nu\delta_{kl}\right)\frac{\partial \epsilon}{\partial x_l}\right] + \tilde{c}(c_{\epsilon 1} + \psi_1 + \psi_2)\frac{\epsilon}{k}P_k - c_{\epsilon 2}\frac{\epsilon\tilde{\epsilon}}{k} \tag{34}$$

with

$$\tilde{\epsilon} \equiv \epsilon - 2\nu\left(\frac{\partial\sqrt{k}}{\partial x_j}\right)^2, \tag{35}$$

$$\psi_1 = 2.5A\left(\frac{P_k}{\epsilon} - 1\right), \tag{36}$$

$$\psi_2 = 0.3(1 - 0.3A_2)\exp[-(0.002Re_t)^2]. \tag{37}$$

The quantity $\tilde{\epsilon}$ equals zero at the wall and, thus, avoids that the last term in Eq. (34) tends to minus infinity as the wall is approached. For the coefficients c_ϵ, $c_{\epsilon 1}$ and $c_{\epsilon 2}$ the standard values of 0.18, 1.45 and 1.9 are taken, respectively. The quantity $\tilde{c}$ is introduced in order to avoid a too strong flow laminarization in the entrance region of the cooled pipe caused by an extremely high local acceleration parameter $K = 20 \div 50 \times 10^{-6}$. For $\tilde{c}$ the following expression is chosen [14]:

$$\tilde{c} = \begin{cases} \exp[-(c_D K)^2] & (K > 0) \\ 1 & (K \le 0) \end{cases} \tag{38}$$

with

$$c_D = \begin{cases} 4.5Re_D & \text{(1. acceleration section)} \\ 3 \times 10^5 & \text{(2. acceleration section)} \end{cases}. \tag{39}$$

For the calculation of the turbulent heat fluxes a simple modelling with the aid of the turbulent Prandtl number is employed. Simulations using transport equations for the turbulent heat fluxes reveal stability problems and do not lead to an improvement concerning the coincidence with the experimental results.

The turbulent heat flux is assumed to be proportional to the turbulent thermal diffusivity

$$\overline{v_r t} = -\nu_q \frac{\partial T}{\partial r} \tag{40}$$

with

$$\nu_q = \frac{\nu_t}{Pr_t} \quad \text{and} \quad \nu_t = c_\nu f_\nu \frac{k^2}{\epsilon}. \tag{41}$$

For the turbulent Prandtl number the value $Pr_t = 0.9$ is chosen and 0.09 is adapted as the value of the constant c_ν. The wall influence is captured by the model function [23]

$$f_\nu = \exp\left(\frac{-3.4}{\left(1 + \frac{Re_t}{50}\right)^2}\right). \tag{42}$$

4.3. Boundary conditions

Boundary conditions have to be provided at the entrance of the cooled section, at the symmetry axis and at the solid–liquid interface:

$$\begin{aligned} &z = 0: \quad V_r = 0; \quad V_z = \text{given}; \quad V_\varphi = 0; \quad P = \text{given}; \\ &\quad T = T_0; \quad \overline{v_i v_j} = \text{given}; \quad \epsilon = \text{given}; \\ &r = 0: \quad V_r = 0; \quad \frac{\partial V_z}{\partial r} = 0; \quad V_\varphi = 0; \quad \frac{\partial T}{\partial r} = 0; \\ &\quad \frac{\partial \overline{v_i v_j}}{\partial r} = 0 (i = j); \quad \overline{v_i v_j} = 0 (i \ne j); \quad \frac{\partial \epsilon}{\partial r} = 0; \\ &r = \delta: \quad V_r = 0; \quad V_z = 0; \quad V_\varphi = \frac{\delta}{R} V_{\varphi w}; \\ &\quad T = T_F; \quad \overline{v_i v_j} = 0; \quad \tilde{\epsilon} = 0. \end{aligned} \tag{43}$$

4.4. Calculation of ice layer geometry

In order to determine the axial distribution of the local free pipe radius $\delta(z)$, the temperature distribution in the solid phase has to be considered. Neglecting axial heat conduction effects and assuming constant properties leads to the following energy equation for the frozen crust:

$$\frac{\partial}{\partial r}\left(r\frac{\partial T_s}{\partial r}\right) = 0. \tag{44}$$

The boundary conditions at the solid–liquid interface and at the cooled wall are given by

$$\begin{aligned} &T_s(r = \delta) = T_F, \\ &T_s(r = R) = T_W. \end{aligned} \tag{45}$$

In order to couple the temperature distributions in the solid and the liquid phase, the energy equation of the solid–liquid interface is required:

$$r=\delta: \quad k_s\frac{\partial T_s}{\partial r}=k_l\frac{\partial T}{\partial r}. \tag{46}$$

By integrating Eq. (44) and using the boundary conditions (Eq. (45)) the temperature distribution and the temperature gradient in the frozen crust can be calculated:

$$\delta\le r\le R: \quad T_s=T_F-(T_F-T_W)\frac{\ln(r/\delta)}{\ln(R/\delta)}, \tag{47}$$

$$\delta\le r\le R: \quad \frac{\partial T_s}{\partial r}=-\frac{1}{r}\,\frac{T_F-T_W}{\ln(R/\delta)}. \tag{48}$$

Inserting the equation for the temperature gradient (48) into the interface energy Eq. (46) yields the required function for δ:

$$\ln\left(\frac{\delta}{R}\right)=\frac{1}{\delta}\,\frac{k_s}{k_l}\,\frac{T_F-T_W}{\left.\frac{\partial T}{\partial r}\right|_{r=\delta}}. \tag{49}$$

4.5. Numerical method

The differential equations are converted into a dimensionless form and solved numerically with the aid of the finite volume method using a nonuniform grid. Here, a staggered-grid formation ensures a higher stability of the equation system [17,18]. In order to provide the boundary conditions at the solid–liquid interface at a constant value of the radial coordinate, it is scaled with the local free pipe radius:

$$\tilde{r}=\frac{r}{\delta}. \tag{50}$$

For the prediction of the solid phase a straight pipe with no solidification is assumed first ($\delta/R=1$). By solving the equation system the temperature gradient along the solid–liquid interface can be calculated providing a new distribution for δ (see Eq. (49)). This iteration procedure is repeated until convergence is achieved—the intensive interaction between the shape of the ice layer and the heat transfer in the flow demands an underrelaxation.

Concerning the calculation of a 'step transition' ice formation with flow separation, the FLARE-approximation [24] ensures the numerical stability in the recirculation region [5].

5. Comparison of experimental and numerical results

5.1. Non-rotating pipe flow

Fig. 10 shows the steady-state shape of the solid phase for $Re_D=20{,}000$, $N=0$ and different freezing parameters. At $B=10$ the ice layer causes only a moderate flow acceleration leading to a 'smooth transition' whereas for $B=13$ a thicker ice layer with 'step transition' occurs.

Fig. 11 elucidates the development of the axial vel-

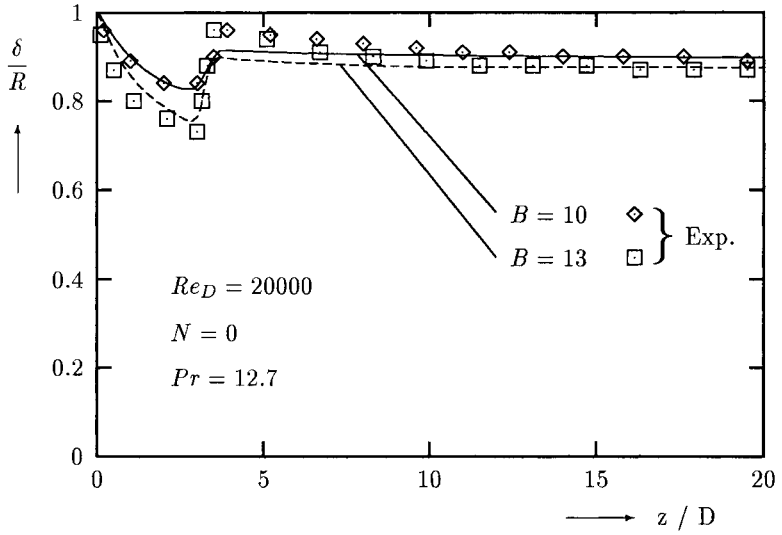

Fig. 10. Ice layers for $Re_D=20{,}000$, $N=0$, $B=10$ ('smooth transition') and $B=13$ ('step transition').

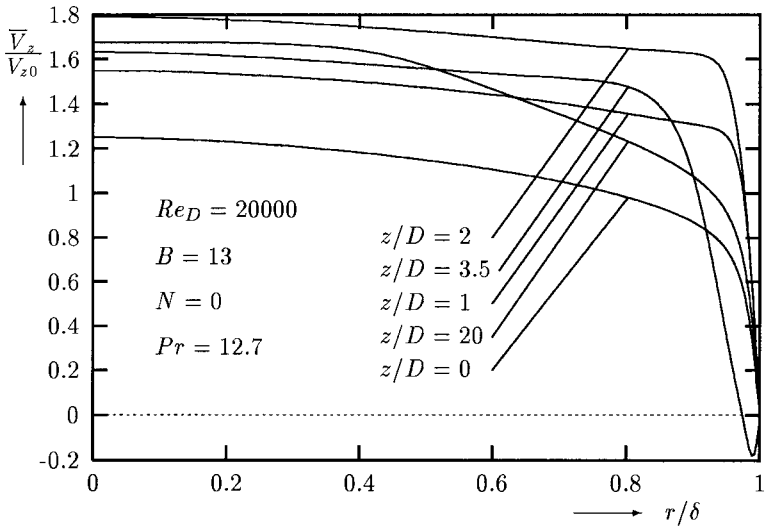

Fig. 11. Development of the axial velocity distribution for $Re_D = 20{,}000$, $B = 13$ and $N = 0$.

ocity distribution for $B = 13$. Due to the convergent ice layer the flow is strongly accelerated in the entrance region ($0 \leq z/D \leq 2$) and approaches a slug profile. In the diffuser section downstream the flow is decelerated and separates from the solid–liquid interface, generating a small recirculation bubble. At the end of the cooled section the ice layer thickness and, therefore, the velocity distributions are nearly constant along the pipe.

Fig. 12 depicts the strong suppression of the streamwise velocity fluctuations $\overline{v_z v_z}$, along the entrance region caused by the flat distribution of V_z leading to a small production term P_{zz} (see Eq. (12)). Moreover, the thickness of the viscous sublayer increases clearly due to a negative production term P_{rr} in the vicinity of the solid–liquid interface [14]. In the diffuser section the velocity gradient $\partial V_z/\partial r$ outside the viscous sublayer increases considerably and generates big production terms P_{zz} and P_{rz}. Therefore, the distribution of $\overline{v_z v_z}$ rises rapidly, too. At the end of the cooled section the flow approaches the state of equilibrium turbulence again.

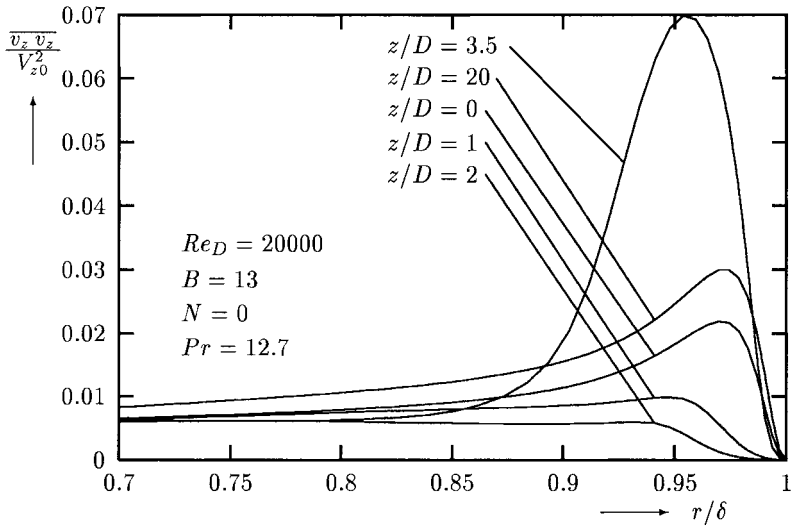

Fig. 12. Development of the streamwise velocity fluctuations for $Re_D = 20{,}000$, $B = 13$ and $N = 0$.

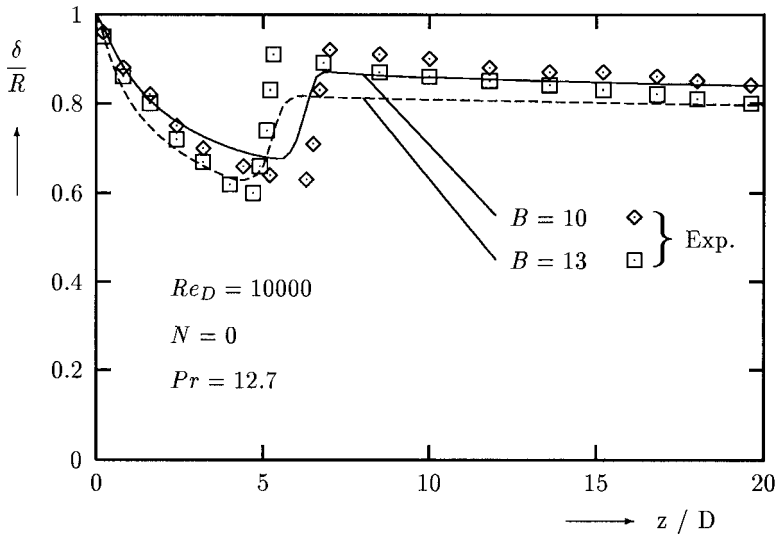

Fig. 13. 'Step transition' Ice layers for $Re_D = 10{,}000$, $N = 0$, $B = 10$ and $B = 13$.

Fig. 13 shows the 'step transition' ice formation for $Re_D = 10{,}000$ and different freezing parameters. At $B = 13$ the wave is located closer to the entrance because the local Reynolds number Re_l increases more rapidly due to the thicker ice layer. This leads to an earlier retransition back to full turbulent flow (see Eq. (5)) and the maximum thickness of the solid phase increases only slightly.

In Fig. 14 one can see the influence of the Reynolds number on the shape of the frozen crust at $B = 18$. At $Re_D = 40{,}000$ the heat transfer rate in the flow is very high and only a quite thin ice layer develops. Thus, the flow laminarization is only moderate and the retransition is introduced faster than in the strongly accelerated flow at $Re_D = 20{,}000$.

All in all, the simulations in Figs. 10, 13 and 14 are in good agreement with the experimental results. Only in the region where the ice layer reaches its minimum thickness the deviations are somewhat larger. This can be explained by the neglect of axial diffusion effects that have a considerable influence on heat transfer in this region. Moreover, for larger diffuser angles the flow is not axisymmetric any more as it is assumed in the theory [5].

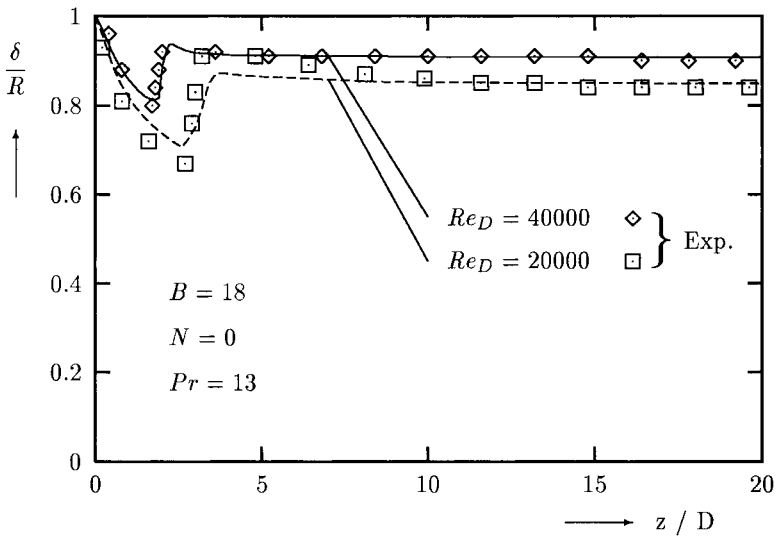

Fig. 14. 'Step transition' Ice layers for $B = 18$, $N = 0$, $Re_D = 20{,}000$ and $Re_D = 40{,}000$.

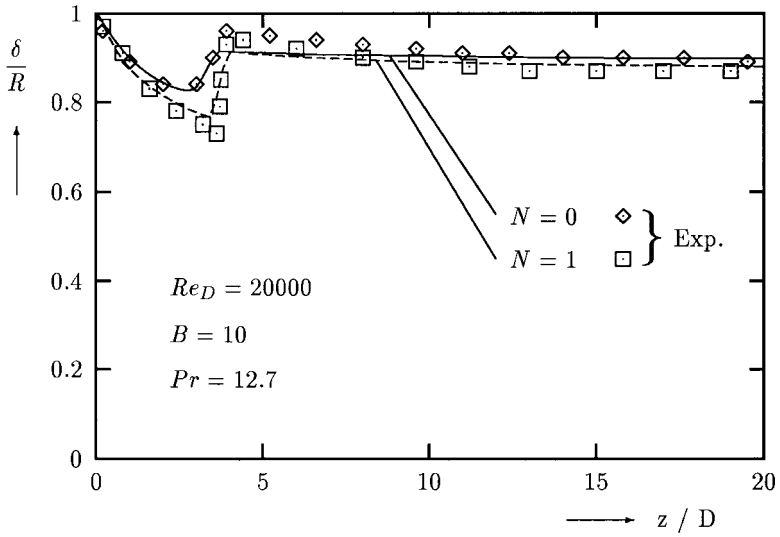

Fig. 15. Ice layers for $Re_D = 20{,}000$, $B = 10$, $N = 0$ ('smooth transition') and $N = 1$ ('step transition').

5.2. Rotating pipe flow

The influence of rotation on the ice layer at $Re_D = 20{,}000$ and $B = 10$ is shown in Fig. 15. At $N = 1$ the additional flow laminarization induced by the rotation causes a thicker solid phase and leads to a 'step transition' ice formation whereas at $N = 0$ a 'smooth transition' occurs.

Fig. 16 depicts the shape of the frozen crust at $Re_D = 10{,}000$, $B = 10$ with rotation ($N = 0.5$) and without ($N = 0$). In the non-rotating pipe the ice layer in the entrance region as well as at the end of the cooled section is thinner, but the maximum thickness occurs at $N = 0$, too. This is caused by the phenomenon that the laminarization effect of rotation decreases rapidly with increasing ice layer thickness (see Eq. (2)). As a result the extreme flow laminarization at $N = 0.5$ is destabilized inducing an early retransition.

Fig. 17 shows the influence of the Reynolds number at $B = 10$ and $N = 0.5$. At the lower value $Re_D = 10{,}000$ the ice layer is thicker again, but in contrast to the conditions in a non-rotating pipe (see Fig. 14) the location of the wave does not depend on the

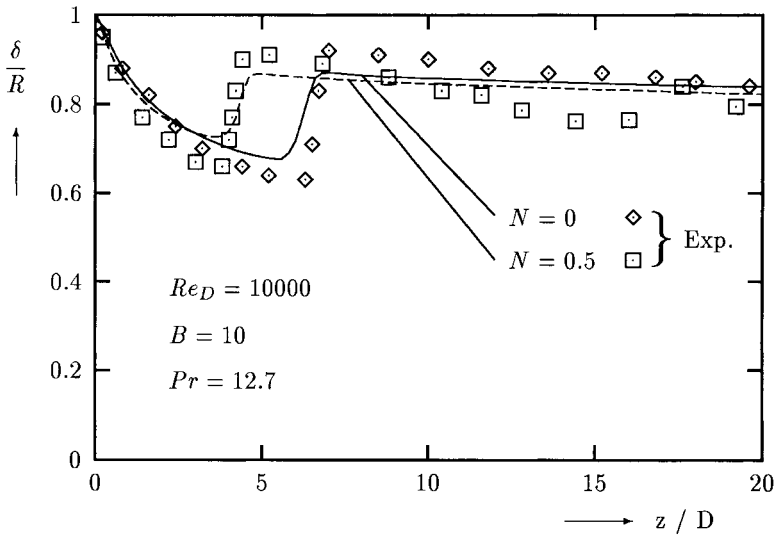

Fig. 16. 'Step transition' ice layers for $Re_D = 10{,}000$, $B = 10$, $N = 0$ and $N = 0.5$.

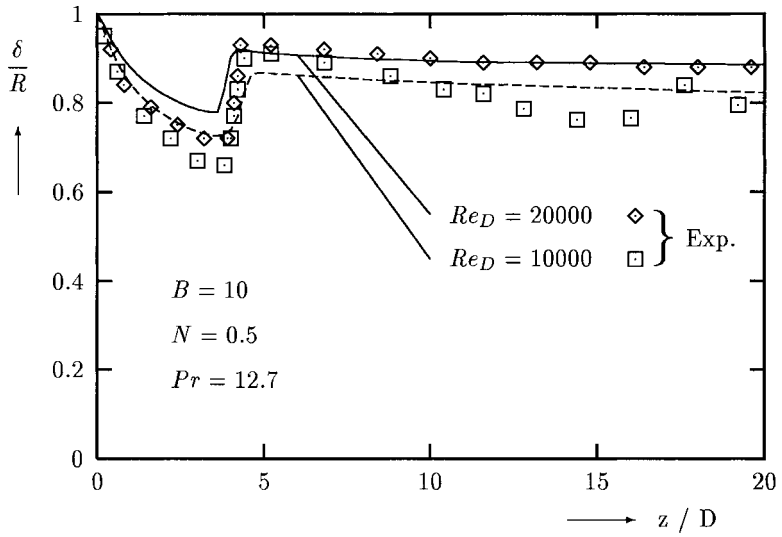

Fig. 17. 'Step transition' ice layers for $B = 10$, $N = 0.5$, $Re_D = 10{,}000$ and $Re_D = 20{,}000$.

Reynolds number any more (see Eq. (6)). Because of the thinner ice layer the laminarization due to rotation decreases slower matching the less intensive turbulence suppression caused by the flow acceleration.

Concerning the effects of pipe rotation the turbulence model provides a very good agreement with experimental results. Only the second wave at $Re_D = 10{,}000$, $B = 10$, $N = 0.5$ (see Figs. 6 and 16) is not captured because the applicability of the parabolic model is restricted to ice layers with only one wave.

6. Conclusions

The formation of the steady-state solid–liquid interface in an axially rotating turbulent pipe flow is influenced by two different laminarization effects. The acceleration of the flow caused by the converging shape of the solid phase leads to a suppression of turbulent motion which is enhanced by the laminarization effect of the superimposed pipe rotation. The subsequent retransition of the flow generates a wavy shape of the frozen crust. Considering a 'step transition' ice formation with flow separation the location of the separation point z_w is found to be a function of the freezing parameter B. Moreover, in the non-rotating pipe the Reynolds number Re_D influences z_w, too.

The applied Reynolds stress turbulence model is able to capture the mentioned laminarization effects and provides a good agreement with experimental ice layers showing one wave.

References

[1] R.D. Zerkle, J.E. Sunderland, The effect of liquid solidification in a tube upon laminar-flow heat transfer and pressure drop, ASME Journal of Heat Transfer 90 (1968) 183–190.

[2] B. Weigand, H. Beer, Freezing in turbulent flow inside tubes and channels, Wärme- und Stoffübertragung 28 (1993) 57–64.

[3] R.R. Gilpin, Ice formation in a pipe containing flows in the transition and turbulent regimes, ASME Journal of Heat Transfer 103 (1981) 363–368.

[4] T. Hirata, H. Matsuzawa, A study of ice-formation phenomena on freezing of flowing water in a pipe, ASME Journal of Heat Transfer 109 (1987) 965–970.

[5] B. Weigand, H. Beer, Ice-formation phenomena for water flow inside a cooled parallel plate channel: an experimental and theoretical investigation of wavy ice layers, International Journal of Heat and Mass Transfer 36 (1993) 685–693.

[6] K. Kikuyama, M. Murakami, K. Nishibori, K. Maeda, Flow in an axially rotating pipe, Bulletin of the JSME 26 (1983) 506–513.

[7] G. Reich, H. Beer, Fluid flow and heat transfer in an axially rotating pipe—I. Effect of rotation on turbulent pipe flow, International Journal of Heat and Mass Transfer 32 (1989) 551–562.

[8] K. Nishibori, K. Kikuyama, M. Murakami, Laminarization of turbulent flow in the inlet region of an axially rotating pipe, Bulletin of the JSME 30 (1987) 255–262.

[9] B. Weigand, H. Beer, Fluid flow and heat transfer in an axially rotating pipe: the rotational entrance, in: Proceedings of the Third International Symposium on Transport Phenomena and Dynamics of Rotating Machinery, Honolulu, Hawaii, 1990, vol. 1. pp. 439–454.

[10] S. Hirai, T. Takagi, M. Matsumoto, Predictions of the laminarization phenomena in an axially rotating pipe flow, ASME Journal of Fluids Engineering 110 (1988) 424–430.
[11] J.M. Eggels, Direct and large eddy simulation of turbulent flow in a cylindrical pipe geometry, Doctoral thesis, Delft University Press, 1994.
[12] K.-J. Rinck, H. Beer, Freezing in turbulent flow inside an axially rotating pipe at low flow-rate Reynolds numbers, in: Proceedings of the Sixth International Symposium on Transport Phenomena and Dynamics of Rotating Machinery, Honolulu, Hawaii, 1996, vol. 2. pp. 440–449.
[13] P.M. Moretti, W.M. Kays, Heat transfer to a turbulent boundary layer with varying free-stream velocity and varying surface temperature—an experimental study, International Journal of Heat and Mass Transfer 8 (1965) 1187–1202.
[14] K.-J. Rinck, Erstarrungsvorgänge einer Flüssigkeit in einem turbulent durchströmten und axial rotierenden Rohr, Doctoral thesis, TU Darmstadt, Fortschritt-Berichte VDI Verlag, Reihe 7, Düsseldorf, 1999.
[15] T. Cebeci, K.C. Chang, A general method for calculating momentum and heat transfer in laminar and turbulent duct flows, Numerical Heat Transfer 1 (1978) 39–68.
[16] T. Rothe, H. Beer, An experimental and numerical investigation of turbulent flow and heat transfer in the entrance region of an annulus between rotating tubes, in: Proceedings of the Fifth International Symposium on Transport Phenomena and Dynamics of Rotating Machinery, Honolulu, Hawaii, 1994, vol. A, pp. 548–560.
[17] S. Hogg, M.A. Leschziner, Computation of highly swirling confined flow with a Reynolds stress turbulence model, AIAA Journal 27 (1989) 57–63.
[18] B.E. Launder, N. Shima, Second-moment closure for the near-wall sublayer: development and application, AIAA Journal 27 (1989) 1319–1325.
[19] K-J. Rinck, H. Beer, Numerical calculation of the fully developed turbulent flow in an axially rotating pipe with a second-moment closure, ASME Journal of Fluids Engineering 120 (1998) 274–279.
[20] J.C. Rotta, Statistische Theorie nichthomogener Turbulenz, Zeitschrift für Physik 129 (1951) 547.
[21] M. Ohtsuka, Numerical analysis of swirling non-reacting and reacting flows by the Reynolds stress differential method, International Journal of Heat and Mass Transfer 38 (1995) 331–337.
[22] B.J. Daly, F.H. Harlow, Transport equations in turbulence, Physics of Fluids 13 (1970) 2634–2649.
[23] B.E. Launder, B.I. Sharma, Application of the energy-dissipation model of turbulence to the calculation of flow near a spinning disk, Letters in Heat and Mass Transfer 1 (1974) 131–137.
[24] T.A. Reyner, I. Flügge-Lotz, The interaction of a shock wave with a boundary layer, International Journal of Nonlinear Mechanics 3 (1968) 173–199.